Title

Understanding and reducing the uncertainties of land surface energy flux partitioning within CMIP6 land models

Authors

Yuan, Kunxiaojia

Zhu, Qing

Riley, William J

et al.

Publication Date

2022-05-01

DOI

10.1016/j.agrformet.2022.108920

Peer reviewed

Agricultural and Forest Meteorology 319 (2022) 108920

Contents lists available at ScienceDirect

Agricultural and Forest Meteorology

journal homepage: www.elsevier.com/locate/agrformet

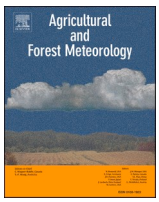

Understanding and reducing the uncertainties of land surface energy flux partitioning within CMIP6 land models

Kunxiaojia Yuan [a,b,*], Qing Zhu [a,*], William J. Riley [a], Fa Li [a,b], Huayi Wu [b]

[a] Climate and Ecosystem Sciences Division, Climate Sciences Department, Lawrence Berkeley National Laboratory, Berkeley, CA, USA
[b] State Key Laboratory of Information Engineering in Surveying, Mapping and Remote Sensing, Wuhan University, Wuhan, China

ARTICLE INFO

Keywords:
Energy fluxes
CMIP6
Uncertainty reduction
Machine learning
Causal inference

ABSTRACT

Land surfaces dissipate energy through latent (*LE*) and sensible (*H*) heat fluxes that modulate atmospheric temperature and humidity, which in return affect land surface vegetation and soil processes. Within this two-way land-atmosphere coupling, surface energy partitioning (*LE* versus *H*) plays a central role in connecting the land and atmosphere states and fluxes. However, considerably large uncertainties still exist in earth system land models, *i.e.* the phase 6 of the Coupled Model Intercomparison Project (CMIP6). Further, the underlying controls from climate and biological factors on surface energy partitioning over different biome types are not well understood. In this study, we combined machine learning (ML) and causal inference models to investigate and reduce the uncertainties (*i.e.*, parametric, structural, and forcing uncertainties) of CMIP6 simulated evaporative fraction (defined as $LE / (LE + H)$) across 64 FLUXNET sites that cover five major biomes. We found that CMIP6 model ensembles overestimated evaporative fraction with considerable spread at deciduous broadleaf forest, evergreen needleleaf forest, and savanna sites. Accounting for the biases from all related surface climate and biological driving variables, the CMIP6 model simulated EF could be largely improved (*e.g., R* between model and observed EF improved from 0.47 to 0.66), with leaf area index, vapor pressure deficit, and precipitation dominated the model improvement. Furthermore, ML-based parameterization generally showed a promising opportunity to further reduce model biases (*e.g., R* improved from 0.66 to 0.80) in spite of the limited improvement at evergreen broadleaf forest sites where model bias may be dominated by structural imperfection. This study provided an effective framework to understand and reduce model uncertainties in simulating land surface energy flux partitioning and, more importantly, highlighted the need of effective model structure improvement for the next generation earth system land model development.

1. Introduction

The land surface and atmosphere are closely coupled through the water, carbon, and energy cycles (Gentine et al., 2019; Santanello Jr et al., 2013), and the coupling is important in both current (Betts, 2009; Ferguson et al., 2012; Koster et al., 2004) and future climate (Dirmeyer et al., 2012; Seneviratne et al., 2006). Land surface latent heat and evapotranspiration fluxes (i.e., transpiration, inland water and soil evaporation, and canopy interception evaporation) modulate atmospheric temperature and moisture content, which in turn affect soil processes and vegetation growth through controls on aerodynamic resistance, soil conditions, and plant stomatal status (Feldman et al., 2019; Lian et al., 2018; Lombardozzi et al., 2015; Williams and Torn, 2015; Yuan et al., 2021). Biases of land surface-atmospheric water and energy partitioning can lead to biases in simulations of air temperature (Teuling et al., 2010; Ukkola et al., 2018), precipitation (Berg et al., 2013; Kaye L Brubaker et al., 1993; Schär et al., 1999), and land surface water, energy, and carbon fluxes (Cai et al., 2019; Williams and Torn, 2015; Zhu et al., 2016). Therefore, the Evaporative Fraction (EF, the ratio of latent heat (LE) flux to the sum of latent and sensible heat (H) fluxes), which defines how the land surface partitions net radiation into LE versus H (Feldman et al., 2019), is valuable when analyzing land-atmosphere coupling (Feldman et al., 2019; Ford et al., 2014; Koster et al., 2009).

Earth system land models have been used to estimate land surface energy partitioning and patterns of land-atmosphere coupling (Koster et al., 2002, 2006; Liu et al., 2019), albeit with acknowledged biases and uncertainties in the analyzed land models (e.g., from the Coupled Model

* Corresponding authors.
E-mail addresses: kunxiaojiayuan@lbl.gov (K. Yuan), qzhu@lbl.gov (Q. Zhu).

https://doi.org/10.1016/j.agrformet.2022.108920
Received 20 September 2021; Received in revised form 28 February 2022; Accepted 24 March 2022
Available online 6 April 2022

Intercomparison Project phase 5 (CMIP5) (Li et al., 2018; Ukkola et al., 2018; Williams et al., 2016)). To this end, significant efforts have been focused on evaluating and parameterizing the land models with, e.g., FLUXNET observations to reduce model-observation discrepancies (Cai et al., 2019; Chen et al., 2010; Lian et al., 2018; Zhu et al., 2016; Zhu and Zhuang, 2015). For example, Cai et al. (2019) improved representation of deforestation induced evapotranspiration changes through optimization of stomatal resistance and soil water parameters. However, traditional land model parameterization required either a large number of ensemble simulations or developing a complex data-assimilation framework (Zhu and Zhuang, 2014).

Besides model parameters, the uncertainties of simulated land surface energy partitioning could stem from climate and biological drivers, which have not been fully investigated for the-state-of-the-art Coupled Model Intercomparison Project phase 6 (CMIP6) models, in spite of the fact that impacts of climate drivers could largely affect the model simulated land surface water and energy fluxes (Lawrence et al., 2019; Liu et al., 2015; Yuan et al., 2021).

In addition, functional structures (e.g., cause-effect relationships) may also contribute to uncertainties in surface energy partitioning (Williams and Torn, 2015). It is challenging to harmonize dominant controllers of modeled versus observed EF patterns at large scale (Tang et al., 2018; Yuan et al., 2021). For example, most studies have emphasized the importance of soil moisture (Dirmeyer, 2011; Feldman et al., 2019; Ford et al., 2014), while some studies showed much stronger controls from vegetation-related factors (i.e., leaf area index) and much weaker correlation between EF and soil states (Tang et al., 2018; Williams et al., 2016; Williams and Torn, 2015). These inconsistencies may result from spatially-variable EF responses to environmental or biological factors (Dirmeyer, 2011) and nonlinearity of the emergent functional structures (Williams and Torn, 2015), which are difficult to detect with commonly-applied linear-correlation-based methods.

Furthermore, confounding effects caused by the interactions among the land-atmosphere-vegetation variables may lead to interferences in understanding the emergent functional structures between EF and driving variables (Brubaker, 1995; Zeng et al., 2002). For example, the correlation between vegetation-related factors (e.g., leaf area index, or gross primary productivity) to EF can be confounded by soil moisture (Hoek van Dijke et al., 2020; Koster et al., 2004), and seasonal covariation may not correspond to a causal relationship as part of the covariation may be attributed to the same seasonal patterns caused by the common drivers (Nelson et al., 2020).

Therefore, a comprehensive evaluation of the (1) parametric, (2) climate forcing, and (3) functional structure uncertainties of modeled EF in state-of-the-art land models is urgently needed, particularly in the context of predicting current and future land-atmosphere coupling. The objectives of this analysis are: (1) evaluating modeled EF from twelve CMIP6 models at 64 FLUXNET eddy covariance sites covering five major biome types; (2) using machine learning based surrogate models to understand and reduce biases from drivers and model parameterization; (3) applying a nonlinear causality inference model to inform the functional structure biases within CMIP6 models.

2. Methodology

2.1. Observation and model datasets

The observation dataset used in this study is from the FLUXNET 2015 Tier 1 (Pastorello et al., 2020). Here, we focused on five biome types: Deciduous Broadleaf Forest (DBF), Evergreen Broadleaf Forest (EBF), Evergreen Needleleaf Forest (ENF), Grassland (GRA), and Savanna (SAV). A total of 64 sites with at least five years of observations for each site were selected (Fig. 1; detailed site descriptions in Table S1). Among the 64 sites, 12 sites were DBF, 5 sites were EBF, 25 sites were ENF, 14 sites were GRA, and 8 sites were SAV. The observed monthly Latent heat (LE) and sensible heat (H) fluxes were used to calculate EF as LE/(LE+H). Here, the energy fluxes were corrected through an energy balance closure correction factor, calculated as (Net Radiation-Ground Heat)/(H+LE) (Pastorello et al., 2020). Details of energy balance closure adjustment can be seen in Pastorello et al. (2020). This method has been widely used in eddy covariance flux data, although there is no general agreement on which approach is the most suitable one for energy balance correction (Mauder et al., 2018; Pastorello et al., 2020). We also included other associated and available observations (from FLUXNET dataset) in our analysis, including gross primary productivity (GPP), air temperature (TA), downwelling shortwave radiation (R), precipitation (Prcp), vapor pressure deficit (VPD), and soil moisture (SWC). Since leaf area index (LAI) has been identified as an important driver of land-atmosphere coupling in previous studies (Hoek van Dijke et al., 2020; Williams and Torn, 2015), we included LAI, derived from the Moderate-Resolution Imaging Spectroradiometer (MODIS) satellite data product MCD15A3H (Myneni et al., 2015), as a potential driver. All aforementioned variables have been reported as potential important drivers for land-atmosphere coupling (Blyth et al., 2019; Feldman et al., 2019; Williams and Torn, 2015; Yuan et al., 2021).

The historical CMIP6 simulations of monthly *LE* and *H* and relevant driving factors were obtained from the CMIP6 archive (https://esgf-node.llnl.gov/projects/cmip6/). Twelve models (AWI-ESM-1-1-LR, EC-Earth3-Veg, NorESM2-LM, NorESM2-MM, SAM0-UNICON, CanESM5,

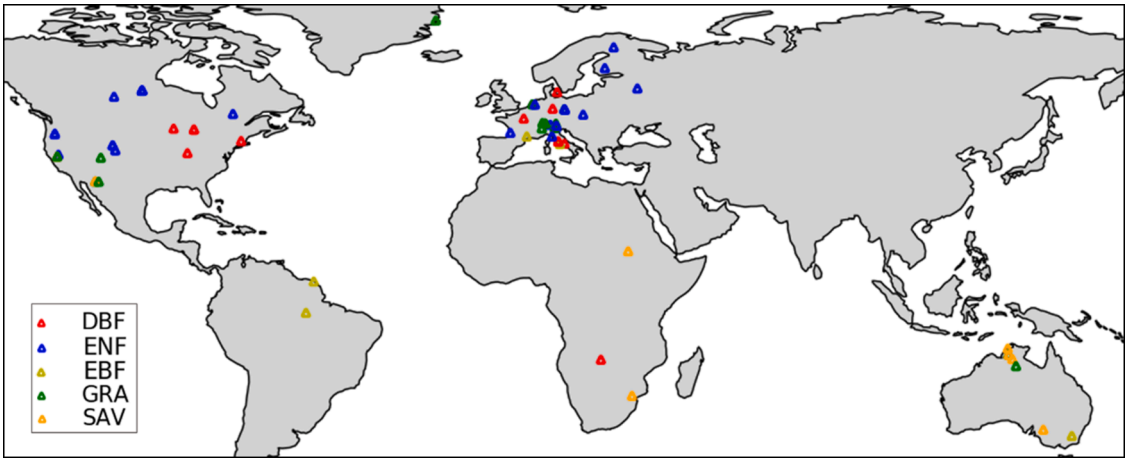

Fig. 1. Location and biome types of selected sites: Deciduous Broadleaf Forest (DBF), Evergreen Broadleaf Forest (EBF), Evergreen Needleleaf Forest (ENF), Grassland (GRA), and Savanna (SAV).

CESM2, CESM2-WACCM, IPSL-CM6A-LR, CMCC-CM2-SR5, GISS-E2-1-G, and GISS-E2-1-H) were selected based on the availability of the diagnostic variables required for this study. Detailed information of CMIP6 models used, including corresponding development institutions, land surface model components and references, is listed in Table S2. For the drivers, LAI, GPP, T, R, Prcp, and SWC can be directly obtained from CMIP6 archives. The monthly VPD was calculated as the difference between the modelled lower-atmosphere saturated vapor pressure and the actual vapor pressure using monthly temperature, surface pressure, and relative humidity (Zhao and Running, 2010). All the CMIP6 outputs were unified to a spatial resolution of 1° × 1° using bi-linear interpolation.

2.2. Surrogate machine learning model

Analyzing the biases from parametric uncertainty and drivers requires data-driven reconstructions of physical models (Lian et al., 2018). In this study, we surrogated each CMIP6 model using an artificial neural network (ANN) (Park et al., 2019; Verrelst et al., 2016) with EF as the target variable. ANN-based surrogate models were trained using each CMIP6 model simulations to best reproduce the model behaviors (Fer et al., 2018; Zhu et al., 2021). This approach has been widely used in earth system science (Reichstein et al., 2019). For each CMIP6 model, we established five ANN-surrogate models, corresponding to the five biome types (Fig. 1). Each ANN model consisted of three hidden layers with 50, 40, and 5 neurons in each layer; with a hyperbolic tangent non-linear activation function (Li et al., 2020; Zamanlooy and Mirhassani, 2013). The surrogate models were first trained with 90% randomly sampled CMIP6 data and validated against the rest 10% of data (Li et al., 2020; Lian et al., 2018). When the surrogate models reasonably fitted the relationships in the original CMIP6 models, the parametric and functional structural biases of original CMIP6 models were also embedded in the surrogate models. After obtaining the surrogate models and calibrating driver biases, we fine-tuned each model using observations, and the performance differences before and after the fine-tuning were used to characterize the benefit of model parameterization (Reichstein et al., 2019; Zhu et al., 2021).

2.3. Functional structure uncertainty analysis

To quantify model functional structure with model outputs, we define the model structure as an "emergent functional relationship" between driving variables and EF. Such relationships can be estimated using a causal inference model (Runge et al., 2019a; Yuan et al., 2021). We used the transfer entropy approach to detect causal controls from climate and biological factors on EF (Schreiber, 2000; Yuan et al., 2021). Transfer entropy, based on Shannon information entropy (Shannon, 1949), measures the amount of information transferred from a source variable to a target variable by excluding shared information between confounders and the target variable. For example, the control from source variables (x) to target variable (y; EF in this case) could be measured by information entropy reduction in the EF when knowing the history of x and excluding effects from confounders (z) (Ruddell and Kumar, 2009):

$$T(x \to y) = \sum_{y_t, z, x_t^{[l]}} p\left(y_t, z, x_t^{[l]}\right) \log_2 \frac{p\left(y_t \middle| \left(z, x_t^{[l]}\right)\right)}{p(y_t|z)} \quad (1)$$

where l is the corresponding time lag of source variable x, and z is the set of confounders for y. In theory, all potential confounders should be considered in Eq. (1). However, in practice, too many confounders will cause high dimensionality and statistical instability issues (Runge et al., 2019a; Yuan et al., 2021). To minimize the interferences from important confounders as well as to avoid high dimensionality, we adaptively considered the strongest confounder of EF through the PCMCI framework (Runge et al., 2019b).

We applied the causal inference method to the five land cover types, with time series length of each type longer than 500 data points. Causal relationship inferred by transfer entropy with such series length was suggested to be generally stable according to Ruddell and Kumar (2009). In addition, we tested the statistical significance of the calculated transfer entropy through shuffled surrogate method (Kantz and Schürmann, 1996). In this approach, we first randomly shuffled source and target time series (100 times) to destroy temporal correlations. Then, the shuffled surrogate transfer entropy $T_s(x_s \to y_s)$ was computed for 100 times. Finally, a one-tailed significance test was applied to determine the 95% confidence level of the transfer entropy (Ruddell and Kumar, 2009). For our causality inference analysis, we detrended the data by removing long-term averaged seasonality, and analyzed the resulting anomalies (Ruddell and Kumar, 2009; Yuan et al., 2021).

3. Results

3.1. Biases in CMIP6 simulated surface energy partitioning

We first compared the simulated evaporative fraction (EF) of twelve CMIP6 models with those derived from the observations across 64 FLUXNET sites. Considerable spread existed in modeled monthly EF (relative differences of observed and modeled EF ranged up to 31%), and models of CMIP6 generally overestimated EF especially when the observed EF values were relatively small (Fig. 2a). Across different biome types, simulated EF values were significantly (passing one-tailed t-tests with P-value<0.05) higher than those of observations for ENF and DBF. The median of simulated EF values in SAV and EBF were also larger than observations (Fig. 2b), even though the differences were not significant (P-value>0.05). For GRA, the differences between observed and simulated EF values were not significant (P-value>0.05). Since EF is the ratio of latent heat (LE) to total heat (LE+H) fluxes, we compared the simulated LE and H with observations. For each biome types, models consistently significantly (P-value<0.05) overestimated LE (Fig. 2c), while the simulated H values were significantly (P-value<0.05) lower

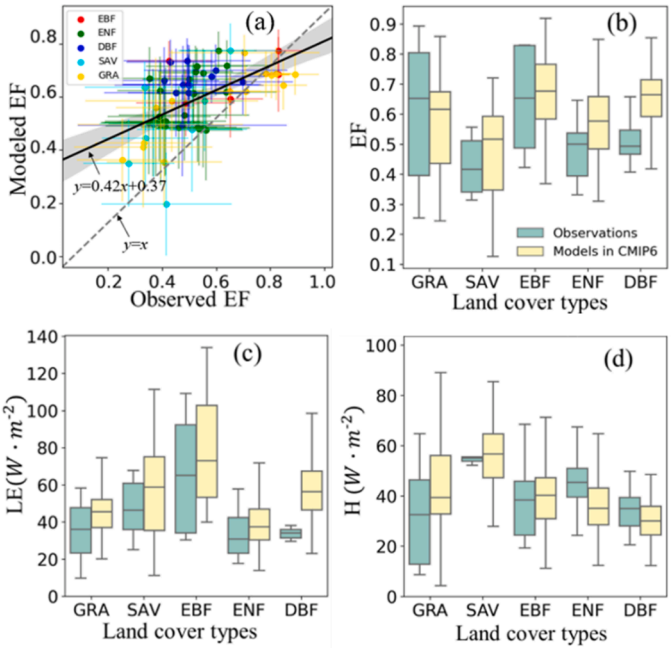

Fig. 2. (a) The site-observed EF values versus the multi-model ensemble mean EF values. Error bars represent site mean and standard deviation. Distribution comparison of the site-observed values versus modeled values over different biome types for (b) evaporative fraction (EF), (c) latent heat (LE), and (d) sensible heat H.

than observations in ENF and DBF, and significantly (P-value<0.05) higher than observations in GRA (Fig. 2d). Generally, models overestimated LE, and EF. The overestimated EF could reduce air temperature through stronger evaporative cooling effects (Ukkola et al., 2018), leading to biases in evapotranspiration, and even precipitation projections in models (Ukkola et al., 2018; Williams and Torn, 2015). To reduce the biases in CMIP6 simulated EF, a deeper understanding of how different sources of biases caused the EF biases is needed. Next, we systematically explored the sources of EF biases from model input drivers, parameterization, and model functional structures for each biome type, considering different land-atmosphere coupling processes across different biome types (Hoek van Dijke et al., 2020).

3.2. Biases from driving variables

To investigate whether biases in drivers significantly caused the overall biases in the modeled EF values, we first developed ANN-surrogated models (Methods), and then replaced the drivers of each model with observations and compared the performance differences before and after changes of drivers. Overall, the ANN-surrogated models reproduced EF values of CMIP6 models reasonably well, explaining 92%-99% of the variance across five biome types (Fig. 3a). Furthermore, by replacing the CMIP6 simulated climate and biological drivers (e.g., TA, GPP) with FLUXNET and MODIS observations, the CMIP6 modeled EF was significantly improved (Fig. 3b, c). For example, the Pearson correlation coefficient (R) between simulated and observed EF values increased from 0.47 (Fig. 3b, P-value<0.05) to 0.66 (Fig. 3c, P-value<0.05) by reducing the uncertainties originating from all climate and biological drivers. Among the drivers, LAI, VPD, and Prcp were the most important three variables in terms of reducing driver caused uncertainties.

The mean absolute error (MAE) at GRA, SAV, and ENF sites were significantly reduced (passing one-tailed t-tests with P-value<0.05), while EBF and DBF showed no significant changes (P-value>0.05) (Fig. 3d). Similarly, R of GRA, SAV, and DBF showed significant improvement while EBF and ENF showed limited changes (not significant, P-value>0.05) (Fig. 3e). The results suggested that generally, correcting the biases of drivers in the CMIP6 models can improve simulated land-atmospheric coupling, especially over GRA and SAV. However, the improvement was limited for EBF. Therefore, investigation of other types of biases (*e.g.*, model structure and parameterization) are needed to further improve model performance.

3.3. Quantifying functional structural biases

The transfer entropy approach was applied to detect relationships between driving variables and EF. We found that GPP had the strongest control on EF in DBF, GRA, and SAV (Fig. 4a, d, e). This result suggested the important role of stomatal controls on ecosystem water loss through evapotranspiration, which is supported by independent analysis on crop biome, grass, and deciduous forest (Williams et al., 2016; Williams and Torn, 2015). Previous studies argued that the observed relationship between GPP and EF might be confounded by the effects from other climate drivers, such as water availability (Koster et al., 2014) or LAI (Tang et al., 2018; Williams et al., 2016). However, in this study, we confirmed the existence of strong controls from GPP by excluding the other dominant confounding effect. Our results showed that the causal controls from LAI are statistically significant, but the strength is much weaker than from GPP, especially in DBF, GRA, and SAV systems (Fig. 4a, d, e). Although both LAI and GPP were commonly used as

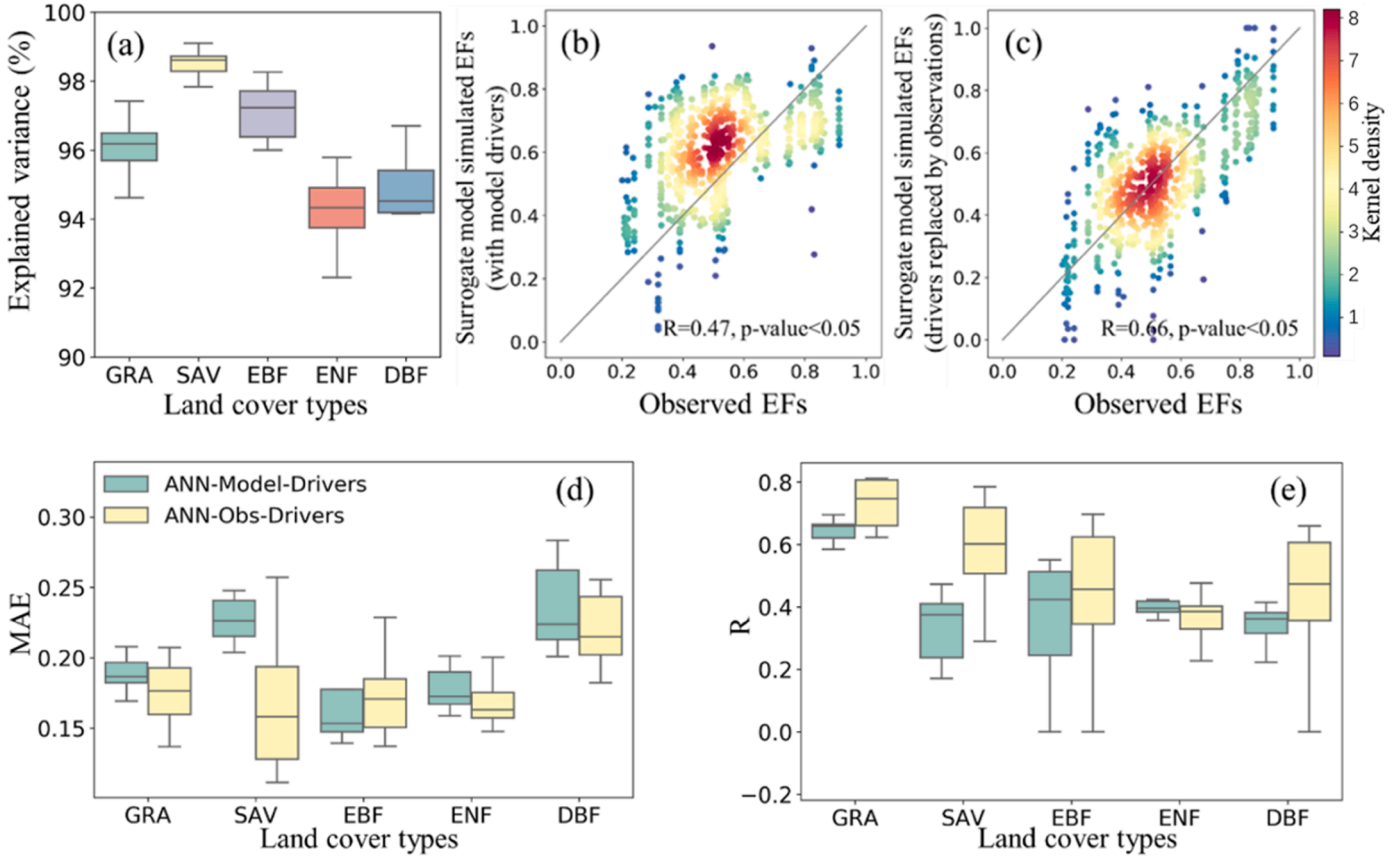

Fig. 3. (a) Explained variance of ANN-surrogate models over five land cover types. (b) Scatterplot of raw CMIP6 EF versus observed EF values. (c) Scatterplot of observed EF versus ANN-modelled EF, but with input drivers replaced by FLUXNET and satellite observations. Performance differences before and after driver calibration in term of (d) mean absolute error (MAE) and (e) Pearson correlation coefficient (R).

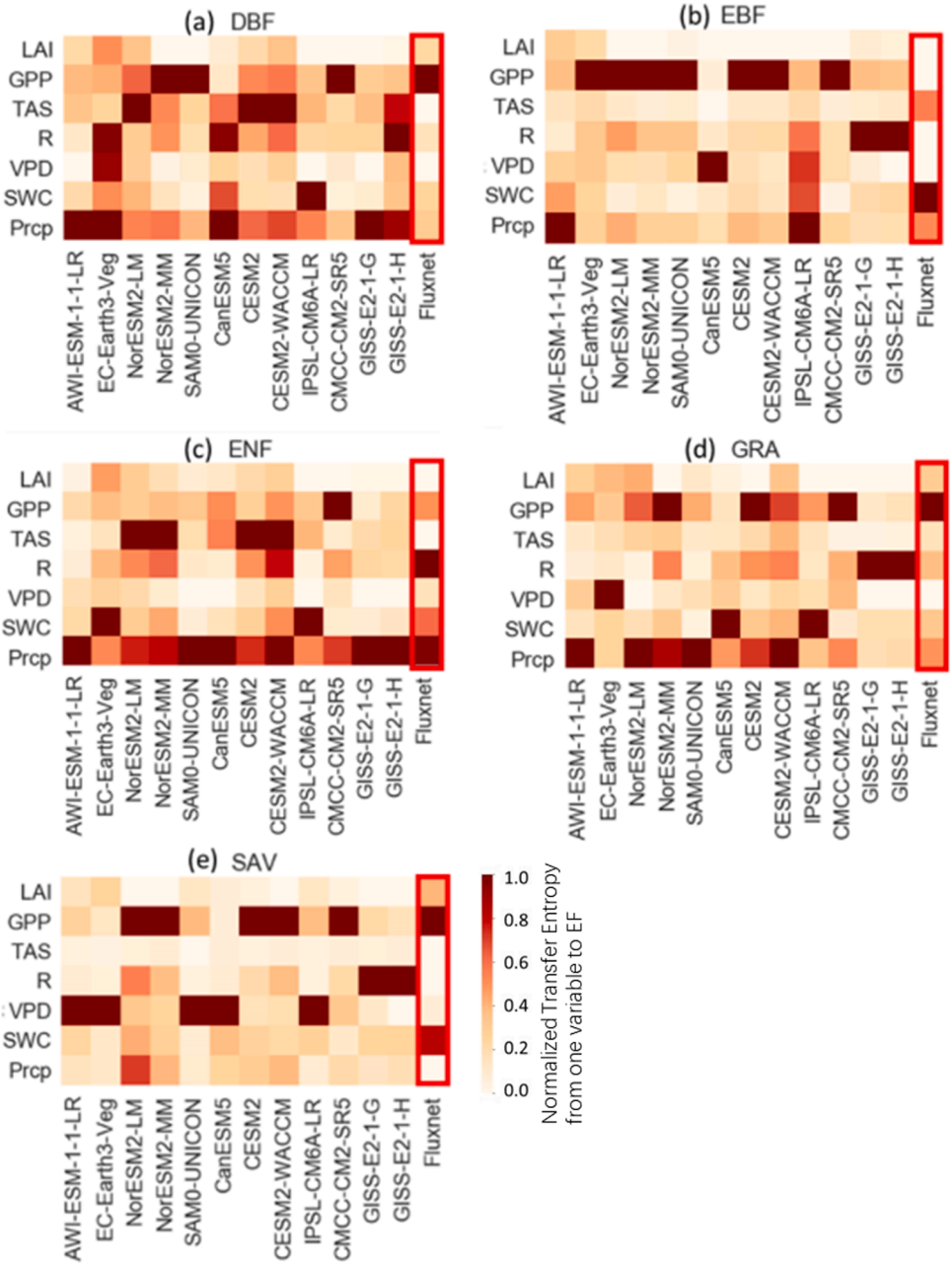

Fig. 4. Controls from climate and biological drivers on EF in FLUXNET observations and CMIP6 models for (a) DBF, (b) EBF, (c) ENF, (d) GRA, and (e) SAV.

proxies of stomatal conductance (Williams and Torn, 2015), GPP and transpiration should be more coupled through direct stomatal control of CO_2 uptake and water loss (Jenerette et al., 2009; Law et al., 2002) than from LAI. Consistently, our results demonstrated that GPP more strongly represents EF variations than LAI. For DBF and GRA, most models underestimated the importance of GPP, and overestimated the importance of water-related variables (*i.e.*, SWC or P) (Fig. 4a and d). For SAV, around half of the models identified the importance of GPP, and the remainder overestimated the impacts from VPD or R (Fig. 4e).

For the ENF sites, R showed a strong relationship with EF in observations, mainly because of the energy limitation over those higher latitude ENF sites (Blyth et al., 2019). However, a majority of the models underestimated the control from R on EF over ENF (Fig. 4c). The water-related factors (SWC or P) also showed important controls on EF in ENF biomes, as confirmed by He et al. (2016) and Hwang et al. (2008). In SAV ecosystems, SWC also played an important role (although weaker than GPP) in regulating EF, which may be due to water limitations (Feldman et al., 2019). All the CMIP6 models underestimated the SWC controls on EF in SAV (Fig. 4e).

For the EBF, observations showed the main control from SWC on EF, while all the models underestimated the impacts from SWC, and most of them represented GPP as the main driver (Fig. 4b). The structural biases in models may be partly caused by the large biases in GPP simulated by CMIP6 models, and such inaccurate simulation of vegetation carbon turnover in EBF has been highlighted in previous studies (Li et al., 2016; Li et al., 2012; Saleska et al., 2003). In this study, large biases and even opposite seasonal cycle (compared with observations) in simulated GPP were also found in EBF sites (such as BR-Sa3 and GF-Guy; Fig. S1), which directly contribute to the large biases in EBF. In terms of the relationship between SWC and EF, whether water-related variables played dominant roles on land surface-atmosphere coupling in EBF still remains controversial in the literature (Baker et al., 2019; Cox et al., 2004; Hoek van Dijke et al., 2020; Lee et al., 2013; Padrón et al., 2017; Saleska et al., 2007). For example, part of the results from models and observations

suggested decreased extent and canopy productivity of EBF because of prominent water limitation (Cox et al., 2004, 2000; Lee et al., 2013), while other results have shown greening-up in EBF despite drought or water-limitation (Huete et al., 2006; Saleska et al., 2007). Part of the reason for the inconsistency may be due to differences in used datasets and methods (Baker et al., 2019), while part of the reason may be related to the spatiotemporally heterogenous responses of EF on changes of climate and biological conditions even for the same biome type (Baker et al., 2019; Blyth et al., 2019) (further discussion can be seen in Section 4.1).

To quantitatively evaluate the differences in model versus observed functional structures, we calculated the cosine similarity (ranges from 0 to 1; (Ye, 2011) to measure structural similarity between models and observations (Fig. 5). A higher value (darker grid) means that the model functional structure is more similar with that of the observation, and vice versa. We found that the similarity metrics varied significantly across different biome types. In general, models showed relatively higher similarity with observations in ENF and GRA (the multi-model average of cosine similarity is 0.74 and 0.73 respectively), while models showed lowest similarity in EBF (the multi-model average of cosine similarity is 0.31). Compared with EBF, although some biome systems (such as GRA and SAV) showed relatively better results in terms of mean cosine similarity, large discrepancies among models existed (cosine similarity ranges from 0.26 to 0.95; Fig. 5) and several models still remained low similarity with observed casual structures (Fig. 5). Model structure differences may be caused by parameterization (Cai et al., 2019; Cuntz et al., 2016) (same physical processes but with different parameter settings) and real structural uncertainty (Wu et al., 2020) (different representation of physical processes).

3.4. Confronting structural biases with parameterization biases

In order to isolate the parameterization biases from real functional structure biases, we tuned the surrogate ANN models using observations (EF and associated driving variables) and evaluated the model performance improvement. We found that the Pearson correlation coefficient (R) between simulated and observed EF values increased from 0.66 (Fig. 3c, P-value<0.05) to 0.80 (Fig. 6a, P-value<0.05) by parameter tuning. For ENF, DBF, and GRA, the performance was significantly (passing one-tailed t-tests with P-value<0.05) improved in terms of MAEs and R through the tuning. While for SAV and EBF, the MAEs were not significantly (P-value>0.05) reduced through parametric tuning, and the R of EBF was significantly (P-value<0.05) lower than that of SAV, implying limited potential benefit of parameterization at EBF sites. Consistently, our causal inference results also showed the lowest structural similarity between models and observations over EBF (Fig. 5), which limited the effectiveness of the model tuning.

4. Discussions

4.1. Varied dominant controllers on surface energy partitioning

It is widely acknowledged that in moisture-limited regions, water-related variables tend to have stronger controls on land surface energy flux partitioning, while in energy-limited areas, radiation tends to be the dominate driver (Teuling et al., 2009; Wang and Dickinson, 2012). For the sites with the same biome type, wetness conditions can vary across different regions (Baker et al., 2019; Hoek van Dijke et al., 2020), which may largely influence the relationship between water-related variables and land surface energy flux partitioning (Baker et al., 2019). For example, for EBF in northwest South America, precipitation is often sufficient throughout the year (Baker et al., 2019), while for EBF in the eastern and southern parts of South America, precipitation is much less (Baker et al., 2019; Goulden et al., 2004), and precipitation variations in water-limited EBF forests can contribute substantially to land-atmosphere coupling (Baker et al., 2019). Our results showed strong controls from SWC on EF in EBF (Fig. 4b), which may be attributed to the relatively drier conditions (Table S3) in studied EBF sites.

Similarly, in ENF, spatiotemporal variations of wetness conditions can also significantly modulate the ratio among different evapotranspiration components (i.e., canopy interception, inland water and soil evaporation, and transpiration) and Bowen ratio (Eltahir, 1998), thus affecting dynamics of land surface energy flux partitioning (Blyth et al., 2019; Raz-Yaseef et al., 2012). Even in water-sufficient ENF systems, strong correlations between precipitation and evapotranspiration were found where interception was nearly as large as transpiration and precipitation variations showed stronger correlation with interception (Blyth et al., 2019). Our results also showed strong controls from water-related variables (i.e., precipitation) on EF in ENF (Fig. 4c), which were consistent with Blyth et al. (2019), and also confirmed by CMIP6 models (Fig. 4c).

Our results showed dominant controls from GPP on EF in DBF, GRA, and SAV (Fig. 4a, d and e), suggesting the important role of vegetations on land-surface energy flux partitioning over these land cover types. Stomatal controls of vegetation directly affect plant transpiration (Bonan, 2008; Seneviratne et al., 2010), which can lead to a strong relationship between GPP (which can be regarded as a proxy of stomatal controls) and EF (Gitelson et al., 2014; Jiang and Ryu, 2016; Mu et al., 2007). For example, Williams et al. (2016) found that the correlation between vegetation activities and EF was around 2~3 times stronger than that from SWC in DBF, GRA, and crop during both relatively drier and wetter periods. During dry periods, vegetation may access soil

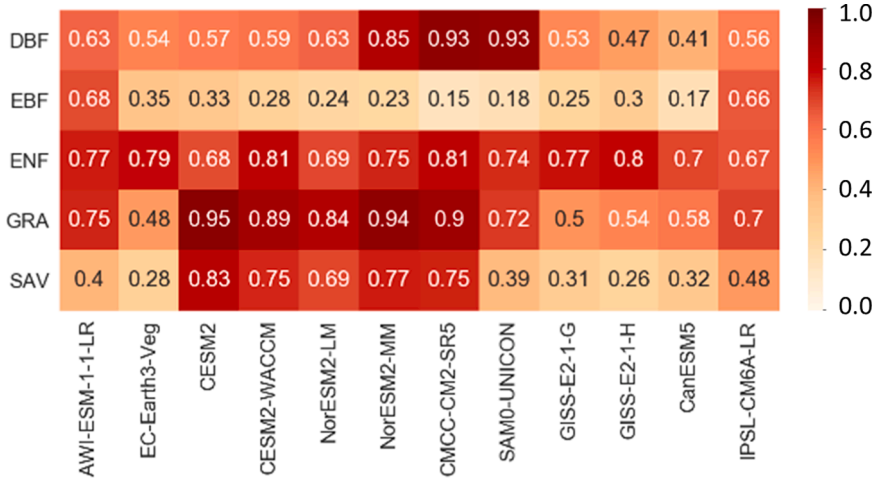

Fig. 5. Cosine similarity of model structure compared with observations. Higher values mean more similar causal structures with that of observed ones.

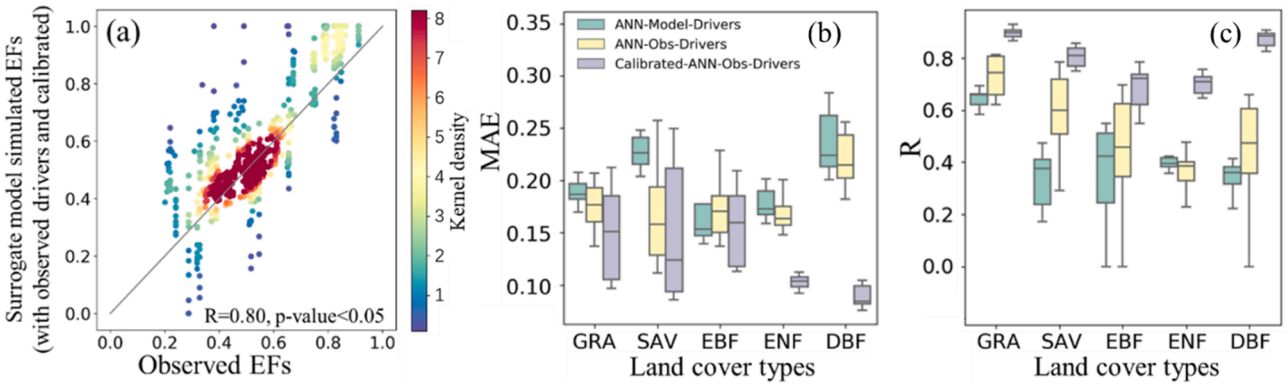

Fig. 6. (a) Scatterplot of EF values of surrogate models with observed drivers and calibrated parameters versus observed EF values. Performance differences before and after driver and parameter calibration in term of (b) mean absolute error (MAE) and (c) Pearson correlation coefficient (R).

moisture from deeper root zone to support transpiration and photosynthesis, with EF not necessarily decreased (Williams et al., 2016); while during wet periods, stomatal conductance may still be curtailed with EF not necessarily increased due to limitation of other unfavorable conditions (e.g., temperature, light, and nutrients) for photosynthesis (Williams et al., 2016). Those results revealed the complexity of multi-factorial influenced processes in land-surface energy flux partitioning (Lawrence et al., 2007; Williams et al., 2016; Yuan et al., 2021).

In summary, our results showed the important roles of water-related variable on land-atmosphere coupling in EBF, ENF, and SAV systems, and dominant controls from GPP on EF in DBF, GRA, and SAV systems. However, given the limited number of sites (especially for EBF with only 5 sites), and large spatial heterogeneity of LAI and wetness conditions across different sites (Hoek van Dijke et al., 2020), we highlight the need to further explore the causal processes in each biome type when more sites and longer observational periods with sufficient drought occurrence are available.

4.2. Similar model performance with the same land component

Models with shared land components generally showed similar model biases after driver and parameterization calibration over the five biome types. Among the twelve CMIP6 models we analyzed, four models (CESM2, CESM2-WACCM, NorESM2-LM, and NorESM2-MM) shared the same land component (CLM5, Table S2). To analyze model structural and performance differences with the same land component, we also included the land-hist simulation of CESM2, which had the same land component (CLM5) but used observational reanalysis datasets (i.e., CRUNCEP) as meteorological forcings. We found that, compared to all ESM models, the EF errors of those models with the same land surface component were narrowed to a relatively smaller range after correcting their biases in drivers and parameterizations (Fig. S2a). Further, models showed similar performance in different biome types (relatively higher R values in DBF, GRA, and SAV; relatively lower R values in EBF and ENF; Fig. S2b). Those results suggested that models with the same land component after driver and parameter calibration, tended to have similar magnitude of errors, which may originate from imperfect structural representations. In addition, we compared causal network similarity between models with the same land components and between models with different land components using cosine similarity (a higher value represents higher similarity) (Ye, 2011). We found that models with the same land component (coupled CESM2, CESM2-WACCM, NorESM2-LM, NorESM2-MM, and CESM2-land-hist) showed significantly (p-value<0.05) higher similarity among their causal networks compared to those with different land components (Figs. S3 and S4). Such causal network similarity patterns highlighted the capability of the causal inference method to identify model structural interdependencies with shared components (Nowack et al., 2020).

4.3. Implications for model development and analysis

EF has been shown to be tightly linked to the characteristics of clouds (Findell and Eltahir, 2003; Schär et al., 1999), air temperature (Teuling et al., 2010; Ukkola et al., 2018), and precipitation (Berg et al., 2013; Brubaker et al., 1993; Schär et al., 1999). Biases of EF representation can result in biases of land surface energy flux (latent heat and sensible heat) partitioning (Williams et al., 2016; Yuan et al., 2021), and further result in biases in climate and weather (e.g., air temperature and precipitation) predictions (Cheruy et al., 2014; Merrifield and Xie, 2016; Williams et al., 2016; Williams and Torn, 2015). Substantial efforts have been invested to parameterize models and reduce model-data discrepancies (Cai et al., 2019; Chen et al., 2010; Decharme, 2007; Meier et al., 2018; Zhu et al., 2016). However, how different types of biases (parametric, driver, and structural biases) affect model performance, has not been fully investigated (Eyring et al., 2019; Yuan et al., 2021), especially for the state-of-the-art CMIP6 models. This study separated influences from each bias source in model performance and explored effectiveness of correcting each bias.

We showed that correcting climate and biological drivers and tuning model parameters are efficient ways to improve model performance in simulating land-atmospheric coupling, especially for GRA, SAV, ENF, and DBF biomes. Models showed limited performance changes through tuning over EBF, which may be attributed to structural imperfections. We therefore highlight the need for more observational benchmarks and model structure development for the EBF biome in the next generation of earth system land models. We also highlight the potential model biases of leaf stomata conductance controls on surface energy partitioning, especially for the DBF, GRA, and SAV, the water-related controls (e.g., precipitation partitioning, soil-related parameters and processes) for ENF and EBF, and the radiation controls (radiation transfer) in ENF.

5. Conclusion

In this study, we analyzed the biases of evaporative fraction (EF) modeled by the state-of-the-art CMIP6 models. We quantitatively estimated the effect of driving variables, parametrization, and structural biases on model performance through ANN-based surrogate model and causal inference. We found that most CMIP6 models overestimated land surface latent heat flux (*LE*) and evaporative fraction (*LE/(LE+H)*) across multiple biome types. Accounting drivers' (e.g., temperature, GPP) uncertainties could significantly improve model performance compared with FLUXNET observations. Further improvement through model tuning towards observations was generally effective, except at evergreen broadleaf forest sites that may be dominated by model structure imperfection. The causal inference results showed that GPP controlled EF at deciduous broadleaf forest, grassland, and savannah ecosystems. While water-related factors (e.g., precipitation, SWC)

showed strong impacts on EF at evergreen needleleaf forest, evergreen broadleaf forest, and savannah ecosystems. And ENF was greatly controlled by solar radiation. This study provided a generic framework to analyze and reduce CMIP6 model biases and highlighted the need for model structure improvements associated with land-atmosphere water and energy fluxes especially at evergreen broadleaf forest ecosystem.

Code availability

The analysis codes used in this paper are available at https://github.com/FaLi-KunxiaojiaYuan/causal-inference-and-machine-learning-for-earth-system-science.

Data availability

The original observed datasets from FLUXNET are available at https://fluxnet.org/. The CMIP datasets are available at https://esgf-node.llnl.gov/projects/cmip6/. The observed LAI variables from MODIS satellite data product MCD15A3H are available at https://lpdaac.usgs.gov/products/mcd15a3hv006/.

Declaration of Competing Interest

The authors declare that they have no known competing financial interests or personal relationships that could have appeared to influence the work reported in this paper.

Acknowledgments

This research was supported by the Reducing Uncertainties in Biogeochemical Interactions through Synthesis and Computation (RUBISCO) Scientific Focus Area and Energy Exascale Earth System Modeling (E3SM, https://e3sm.org/) Project, Office of Biological and Environmental Research of the U.S. Department of Energy Office of Science. Lawrence Berkeley National Laboratory (LBNL) is managed by the University of California for the U.S. Department of Energy under contract DE-AC02-05CH11231.

Supplementary materials

Supplementary material associated with this article can be found, in the online version, at doi:10.1016/j.agrformet.2022.108920.

References

Baker, I.T., Denning, A.S., Dazlich, D.A., Harper, A.B., Branson, M.D., Randall, D.A., Phillips, M.C., Haynes, K.D., Gallup, S.M., 2019. Surface-atmosphere coupling scale, the fate of water, and ecophysiological function in a Brazilian forest. J. Adv. Model. Earth Syst. 11 (8), 2523–2546.

Berg, A., Findell, K., Lintner, B.R., Gentine, P., Kerr, C., 2013. Precipitation sensitivity to surface heat fluxes over North America in reanalysis and model data. J. Hydrometeorol. 14 (3), 722–743.

Betts, A.K., 2009. Land-surface-atmosphere coupling in observations and models. J. Adv. Model. Earth Syst. 1 (3).

Blyth, E.M., Martinez-de la Torre, A., Robinson, E.L., 2019. Trends in evapotranspiration and its drivers in Great Britain: 1961 to 2015. Prog. Phys. Geogr. Earth Environ. 43 (5), 666–693.

Bonan, G.B., 2008. Forests and climate change: forcings, feedbacks, and the climate benefits of forests. Science 320 (5882), 1444–1449.

Brubaker, K.L., 1995. Nonlinear Dynamics of Water and Energy Balance in Land-Atmosphere Interaction. Massachusetts Institute of Technology.

Brubaker, K.L., Entekhabi, D., Eagleson, P., 1993. Estimation of continental precipitation recycling. J. Clim. 6 (6), 1077–1089.

Cai, X., Riley, W.J., Zhu, Q., Tang, J., Zeng, Z., Bisht, G., Randerson, J.T., 2019. Improving representation of deforestation effects on evapotranspiration in the E3SM land model. J. Adv. Model. Earth Syst. 11 (8), 2412–2427.

Chen, Y., Yang, K., Zhou, D., Qin, J., Guo, X., 2010. Improving the Noah land surface model in arid regions with an appropriate parameterization of the thermal roughness length. J. Hydrometeorol. 11 (4), 995–1006.

Cheruy, F., Dufresne, J., Hourdin, F., Ducharne, A., 2014. Role of clouds and land-atmosphere coupling in midlatitude continental summer warm biases and climate change amplification in CMIP5 simulations. Geophys. Res. Lett. 41 (18), 6493–6500.

Cox, P.M., Betts, R., Collins, M., Harris, P.P., Huntingford, C., Jones, C., 2004. Amazonian forest dieback under climate-carbon cycle projections for the 21st century. Theor. Appl. Climatol. 78 (1), 137–156.

Cox, P.M., Betts, R.A., Jones, C.D., Spall, S.A., Totterdell, I.J., 2000. Acceleration of global warming due to carbon-cycle feedbacks in a coupled climate model. Nature 408 (6809), 184–187.

Cuntz, M., Mai, J., Samaniego, L., Clark, M., Wulfmeyer, V., Branch, O., Attinger, S., Thober, S., 2016. The impact of standard and hard-coded parameters on the hydrologic fluxes in the Noah-MP land surface model. J. Geophys. Res. Atmos. 121 (18), 10676–10700.

Decharme, B., 2007. Influence of runoff parameterization on continental hydrology: comparison between the Noah and the ISBA land surface models. J. Geophys. Res. Atmos. 112 (D19108) https://doi.org/10.1029/2007JD008463.

Dirmeyer, P.A., 2011. The terrestrial segment of soil moisture–climate coupling. Geophys. Res. Lett. 38 (16).

Dirmeyer, P.A., Cash, B.A., Kinter, J.L., Stan, C., Jung, T., Marx, L., Towers, P., Wedi, N., Adams, J.M., Altshuler, E.L., 2012. Evidence for enhanced land–atmosphere feedback in a warming climate. J. Hydrometeorol. 13 (3), 981–995.

Eltahir, E.A., 1998. A soil moisture–rainfall feedback mechanism: 1. Theory and observations. Water Resour. Res. 34 (4), 765–776.

Eyring, V., Cox, P.M., Flato, G.M., Gleckler, P.J., Abramowitz, G., Caldwell, P., Collins, W.D., Gier, B.K., Hall, A.D., Hoffman, F.M., 2019. Taking climate model evaluation to the next level. Nat. Clim. Change 9 (2), 102–110.

Feldman, A.F., Short Gianotti, D.J., Trigo, I.F., Salvucci, G.D., Entekhabi, D., 2019. Satellite-based assessment of land surface energy partitioning–soil moisture relationships and effects of confounding variables. Water Resour. Res. 55 (12), 10657–10677.

Fer, I., Kelly, R., Moorcroft, P.R., Richardson, A.D., Cowdery, E.M., Dietze, M.C., 2018. Linking big models to big data: efficient ecosystem model calibration through Bayesian model emulation. Biogeosciences 15 (19), 5801–5830.

Ferguson, C.R., Wood, E.F., Vinukollu, R.K., 2012. A global intercomparison of modeled and observed land–atmosphere coupling. J. Hydrometeorol. 13 (3), 749–784.

Findell, K.L., Eltahir, E.A., 2003. Atmospheric controls on soil moisture–boundary layer interactions. Part I: framework development. J. Hydrometeorol. 4 (3), 552–569.

Ford, T.W., Wulff, C.O., Quiring, S.M., 2014. Assessment of observed and model-derived soil moisture-evaporative fraction relationships over the United States Southern great plains. J. Geophys. Res. Atmos. 119 (11), 6279–6291.

Gentine, P., Green, J.K., Guérin, M., Humphrey, V., Seneviratne, S.I., Zhang, Y., Zhou, S., 2019. Coupling between the terrestrial carbon and water cycles—a review. Environ. Res. Lett. 14 (8), 083003.

Gitelson, A.A., Peng, Y., Arkebauer, T.J., Schepers, J., 2014. Relationships between gross primary production, green LAI, and canopy chlorophyll content in maize: Implications for remote sensing of primary production. Remote Sens. Environ. 144, 65–72.

Goulden, M.L., Miller, S.D., Da Rocha, H.R., Menton, M.C., de Freitas, H.C., e Silva Figueira, A.M., de Sousa, C.A.D., 2004. Diel and seasonal patterns of tropical forest CO_2 exchange. Ecol. Appl. 14 (sp4), 42–54.

He, M., Kimball, J.S., Running, S., Ballantyne, A., Guan, K., Huemmrich, F., 2016. Satellite detection of soil moisture related water stress impacts on ecosystem productivity using the MODIS-based photochemical reflectance index. Remote Sens. Environ. 186, 173–183.

Hoek van Dijke, A.J., Mallick, K., Schlerf, M., Machwitz, M., Herold, M., Teuling, A.J., 2020. Examining the link between vegetation leaf area and land–atmosphere exchange of water, energy, and carbon fluxes using FLUXNET data. Biogeosciences 17 (17), 4443–4457.

Huete, A.R., Didan, K., Shimabukuro, Y.E., Ratana, P., Saleska, S.R., Hutyra, L.R., Yang, W., Nemani, R.R., Myneni, R., 2006. Amazon rainforests green-up with sunlight in dry season. Geophys. Res. Lett. 33 (6).

Hwang, T., Kang, S., Kim, J., Kim, Y., Lee, D., Band, L., 2008. Evaluating drought effect on MODIS gross primary production (GPP) with an eco-hydrological model in the mountainous forest, East Asia. Glob. Change Biol. 14 (5), 1037–1056.

Jenerette, G., Scott, R., Barron-Gafford, G., Huxman, T., 2009. Gross primary production variability associated with meteorology, physiology, leaf area, and water supply in contrasting woodland and grassland semiarid riparian ecosystems. J. Geophys. Res. Biogeosci. 114 (G4).

Jiang, C., Ryu, Y., 2016. Multi-scale evaluation of global gross primary productivity and evapotranspiration products derived from breathing earth system simulator (BESS). Remote Sens. Environ. 186, 528–547.

Kantz, H., Schürmann, T., 1996. Enlarged scaling ranges for the KS-entropy and the information dimension. Chaos Interdiscip. J. Nonlinear Sc. 6 (2), 167–171.

Koster, R., Schubert, S., Suarez, M., 2009. Analyzing the concurrence of meteorological droughts and warm periods, with implications for the determination of evaporative regime. J. Clim. 22 (12), 3331–3341.

Koster, R.D., Dirmeyer, P.A., Guo, Z., Bonan, G., Chan, E., Cox, P., Gordon, C., Kanae, S., Kowalczyk, E., Lawrence, D., 2004. Regions of strong coupling between soil moisture and precipitation. Science 305 (5687), 1138–1140.

Koster, R.D., Dirmeyer, P.A., Hahmann, A.N., Ijpelaar, R., Tyahla, L., Cox, P., Suarez, M. J., 2002. Comparing the degree of land–atmosphere interaction in four atmospheric general circulation models. J. Hydrometeorol. 3 (3), 363–375.

Koster, R.D., Sud, Y., Guo, Z., Dirmeyer, P.A., Bonan, G., Oleson, K.W., Chan, E., Verseghy, D., Cox, P., Davies, H., 2006. GLACE: the global land–atmosphere coupling experiment. Part I: overview. J. Hydrometeorol. 7 (4), 590–610.

Koster, R.D., Walker, G.K., Collatz, G.J., Thornton, P.E., 2014. Hydroclimatic controls on the means and variability of vegetation phenology and carbon uptake. J. Clim. 27 (14), 5632–5652.

Law, B., Falge, E., Gu, L.v., Baldocchi, D., Bakwin, P., Berbigier, P., Davis, K., Dolman, A., Falk, M., Fuentes, J., 2002. Environmental controls over carbon dioxide and water vapor exchange of terrestrial vegetation. Agric. For. Meteorol. 113 (1-4), 97–120.
Lawrence, D.M., Fisher, R.A., Koven, C.D., Oleson, K.W., Swenson, S.C., Bonan, G., Collier, N., Ghimire, B., Van Kampenhout, L., Kennedy, D., 2019. The community land model version 5: description of new features, benchmarking, and impact of forcing uncertainty. J. Adv. Model. Earth Syst. 11 (12), 4245–4287.
Lawrence, D.M., Thornton, P.E., Oleson, K.W., Bonan, G.B., 2007. The partitioning of evapotranspiration into transpiration, soil evaporation, and canopy evaporation in a GCM: Impacts on land–atmosphere interaction. J. Hydrometeorol. 8 (4), 862–880.
Lee, J.E., Frankenberg, C., van der Tol, C., Berry, J.A., Guanter, L., Boyce, C.K., Fisher, J. B., Morrow, E., Worden, J.R., Asefi, S., 2013. Forest productivity and water stress in amazonia: observations from GOSAT chlorophyll fluorescence. Proc. R. Soc. B Biol. Sci. 280 (1761), 20130171.
Li, F., Gui, Z., Zhang, Z., Peng, D., Tian, S., Yuan, K., Sun, Y., Wu, H., Gong, J., Lei, Y., 2020. A hierarchical temporal attention-based LSTM encoder-decoder model for individual mobility prediction. Neurocomputing 403, 153–166.
Li, J., Wang, Y.P., Duan, Q., Lu, X., Pak, B., Wiltshire, A., Robertson, E., Ziehn, T., 2016. Quantification and attribution of errors in the simulated annual gross primary production and latent heat fluxes by two global land surface models. J. Adv. Model. Earth Syst. 8 (3), 1270–1288.
Li, L., Wang, Y., Arora, V.K., Eamus, D., Shi, H., Li, J., Cheng, L., Cleverly, J., Hajima, T., Ji, D., 2018. Evaluating global land surface models in CMIP5: analysis of ecosystem water-and light-use efficiencies and rainfall partitioning. J. Clim. 31 (8), 2995–3008.
Li, L., Wang, Y.P., Yu, Q., Pak, B., Eamus, D., Yan, J., van Gorsel, E., Baker, I.T., 2012. Improving the responses of the Australian community land surface model (CABLE) to seasonal drought. J. Geophys. Res. Biogeosci. 117 (G4).
Lian, X., Piao, S., Huntingford, C., Li, Y., Zeng, Z., Wang, X., Ciais, P., McVicar, T.R., Peng, S., Ottle, C., 2018. Partitioning global land evapotranspiration using CMIP5 models constrained by observations. Nat. Clim. Change 8 (7), 640–646.
Liu, B.Y., Zhu, Q., Riley, W.J., Zhao, L., Ma, H., Van Gordon, M., Larsen, L., 2019. Using information theory to evaluate directional precipitation interactions over the West Sahel region in observations and models. J. Geophys. Res. Atmos. 124 (3), 1463–1473.
Liu, Y., Zhuang, Q., Miralles, D., Pan, Z., Kicklighter, D., Zhu, Q., He, Y., Chen, J., Tchebakova, N., Sirin, A., 2015. Evapotranspiration in Northern Eurasia: impact of forcing uncertainties on terrestrial ecosystem model estimates. J. Geophys. Res. Atmos. 120 (7), 2647–2660.
Lombardozzi, D.L., Bonan, G.B., Smith, N.G., Dukes, J.S., Fisher, R.A., 2015. Temperature acclimation of photosynthesis and respiration: a key uncertainty in the carbon cycle-climate feedback. Geophys. Res. Lett. 42 (20), 8624–8631.
Mauder, M., Genzel, S., Fu, J., Kiese, R., Soltani, M., Steinbrecher, R., Zeeman, M., Banerjee, T., De Roo, F., Kunstmann, H., 2018. Evaluation of energy balance closure adjustment methods by independent evapotranspiration estimates from lysimeters and hydrological simulations. Hydrol. Process. 32 (1), 39–50.
Meier, R., Davin, E.L., Lejeune, Q., Hauser, M., Li, Y., Martens, B., Schultz, N.M., Sterling, S., Thiery, W., 2018. Evaluating and improving the community land model's sensitivity to land cover. Biogeosciences 15 (15), 4731–4757.
Merrifield, A.L., Xie, S.P., 2016. Summer US surface air temperature variability: controlling factors and AMIP simulation biases. J. Clim. 29 (14), 5123–5139.
Mu, Q., Heinsch, F.A., Zhao, M., Running, S.W., 2007. Development of a global evapotranspiration algorithm based on MODIS and global meteorology data. Remote Sens. Environ. 111 (4), 519–536.
Myneni, R., Knyazikhin, Y., Park, T. (2015). MCD15A2H MODIS/Terra+Aqua Leaf Area Index/FPAR 8-day L4 Global 500m SIN Grid V006. NASA EOSDIS Land Processes DAAC. http://doi.org/10.5067/MODIS/MCD15A2H.006.
Nelson, J.A., Pérez-Priego, O., Zhou, S., Poyatos, R., Zhang, Y., Blanken, P.D., Gimeno, T. E., Wohlfahrt, G., Desai, A.R., Gioli, B., 2020. Ecosystem transpiration and evaporation: insights from three water flux partitioning methods across FLUXNET sites. Glob. Change Biol. 26 (12), 6916–6930.
Nowack, P., Runge, J., Eyring, V., Haigh, J.D., 2020. Causal networks for climate model evaluation and constrained projections. Nat. Commun. 11 (1), 1–11.
Padrón, R.S., Gudmundsson, L., Greve, P., Seneviratne, S.I., 2017. Large-scale controls of the surface water balance over land: Insights from a systematic review and meta-analysis. Water Resour. Res. 53 (11), 9659–9678.
Park, S., Shin, J., Kim, S., Oh, E., Kim, Y., 2019. Global climate simulated by the seoul national university atmosphere model version 0 with a unified convection scheme (SAM0-UNICON). J. Clim. 32 (10), 2917–2949.
Pastorello, G., Trotta, C., Canfora, E., Chu, H., Christianson, D., Cheah, Y.W., Poindexter, C., Chen, J., Elbashandy, A., Humphrey, M., 2020. The FLUXNET2015 dataset and the ONEFlux processing pipeline for eddy covariance data. Sci. Data 7 (1), 1–27.
Raz-Yaseef, N., Yakir, D., Schiller, G., Cohen, S., 2012. Dynamics of evapotranspiration partitioning in a semi-arid forest as affected by temporal rainfall patterns. Agric. For. Meteorol. 157, 77–85.
Reichstein, M., Camps-Valls, G., Stevens, B., Jung, M., Denzler, J., Carvalhais, N., 2019. Deep learning and process understanding for data-driven Earth system science. Nature 566 (7743), 195–204.
Ruddell, B.L., Kumar, P., 2009. Ecohydrologic process networks: 1. Identification. Water Resour. Res. 45 (3).
Runge, J., Bathiany, S., Bollt, E., Camps-Valls, G., Coumou, D., Deyle, E., Glymour, C., Kretschmer, M., Mahecha, M.D., Muñoz-Marí, J., 2019a. Inferring causation from time series in Earth system sciences. Nat. Commun. 10 (1), 1–13.
Runge, J., Nowack, P., Kretschmer, M., Flaxman, S., Sejdinovic, D., 2019b. Detecting and quantifying causal associations in large nonlinear time series datasets. Sci. Adv. 5 (11), eaau4996.
Saleska, S.R., Didan, K., Huete, A.R., Da Rocha, H.R., 2007. Amazon forests green-up during 2005 drought. Science 318 (5850), 612. -612.
Saleska, S.R., Miller, S.D., Matross, D.M., Goulden, M.L., Wofsy, S.C., Da Rocha, H.R., De Camargo, P.B., Crill, P., Daube, B.C., De Freitas, H.C., 2003. Carbon in amazon forests: unexpected seasonal fluxes and disturbance-induced losses. Science 302 (5650), 1554–1557.
Santanello, J.A., Peters-Lidard, C.D., Kennedy, A., Kumar, S.V., 2013. Diagnosing the nature of land–atmosphere coupling: a case study of dry/wet extremes in the US Southern great plains. J. Hydrometeorol. 14 (1), 3–24.
Schär, C., Lüthi, D., Beyerle, U., Heise, E., 1999. The soil–precipitation feedback: a process study with a regional climate model. J. Clim. 12 (3), 722–741.
Schreiber, T., 2000. Measuring information transfer. Phys. Rev. Lett. 85 (2), 461.
Seneviratne, S.I., Corti, T., Davin, E.L., Hirschi, M., Jaeger, E.B., Lehner, I., Orlowsky, B., Teuling, A.J., 2010. Investigating soil moisture–climate interactions in a changing climate: a review. Earth Sci. Rev. 99 (3-4), 125–161.
Seneviratne, S.I., Lüthi, D., Litschi, M., Schär, C., 2006. Land–atmosphere coupling and climate change in Europe. Nature 443 (7108), 205–209.
Shannon, C.E., 1949. Communication theory of secrecy systems. Bell Syst. Tech. J. 28 (4), 656–715.
Tang, Q., Xie, S., Zhang, Y., Phillips, T.J., Santanello, J.A., Cook, D.R., Riihimaki, L.D., Gaustad, K.L., 2018. Heterogeneity in warm-season land-atmosphere coupling over the US Southern great plains. J. Geophys. Res. Atmos. 123 (15), 7867–7882.
Teuling, A.J., Hirschi, M., Ohmura, A., Wild, M., Reichstein, M., Ciais, P., Buchmann, N., Ammann, C., Montagnani, L., Richardson, A., 2009. A regional perspective on trends in continental evaporation. Geophys. Res. Lett. 36 (2).
Teuling, A.J., Seneviratne, S.I., Stöckli, R., Reichstein, M., Moors, E., Ciais, P., Luyssaert, S., Van Den Hurk, B., Ammann, C., Bernhofer, C., 2010. Contrasting response of European forest and grassland energy exchange to heatwaves. Nat. Geosci. 3 (10), 722–727.
Ukkola, A., Pitman, A., Donat, M., De Kauwe, M., Angélil, O., 2018. Evaluating the contribution of land-atmosphere coupling to heat extremes in CMIP5 models. Geophys. Res. Lett. 45 (17), 9003–9012.
Verrelst, J., Sabater, N., Rivera, J.P., Muñoz-Marí, J., Vicent, J., Camps-Valls, G., Moreno, J., 2016. Emulation of leaf, canopy and atmosphere radiative transfer models for fast global sensitivity analysis. Remote Sens. 8 (8), 673.
Wang, K., Dickinson, R.E., 2012. A review of global terrestrial evapotranspiration: observation, modeling, climatology, and climatic variability. Rev. Geophys. 50 (2).
Williams, I.N., Lu, Y., Kueppers, L.M., Riley, W.J., Biraud, S.C., Bagley, J.E., Torn, M.S., 2016. Land-atmosphere coupling and climate prediction over the US Southern great plains. J. Geophys. Res. Atmos. 121 (20), 12125–112144.
Williams, I.N., Torn, M.S., 2015. Vegetation controls on surface heat flux partitioning, and land-atmosphere coupling. Geophys. Res. Lett. 42 (21), 9416–9424.
Wu, G., Cai, X., Keenan, T.F., Li, S., Luo, X., Fisher, J.B., Cao, R., Li, F., Purdy, A.J., Zhao, W., 2020. Evaluating three evapotranspiration estimates from model of different complexity over China using the ILAMB benchmarking system. J. Hydrol. 590, 125553.
Ye, J., 2011. Cosine similarity measures for intuitionistic fuzzy sets and their applications. Math. Comput. Modell. 53 (1-2), 91–97.
Yuan, K., Zhu, Q., Zheng, S., Zhao, L., Chen, M., Riley, W.J., Cai, X., Ma, H., Li, F., Wu, H., 2021. Deforestation reshapes land-surface energy-flux partitioning. Environ. Res. Lett. 16 (2), 024014.
Zamanlooy, B., Mirhassani, M., 2013. Efficient VLSI implementation of neural networks with hyperbolic tangent activation function. IEEE Trans. Very Large Scale Integr. VLSI Syst. 22 (1), 39–48.
Zeng, N., Hales, K., Neelin, J.D., 2002. Nonlinear dynamics in a coupled vegetation–atmosphere system and implications for desert–forest gradient. J. Clim. 15 (23), 3474–3487.
Zhao, M., Running, S.W., 2010. Drought-induced reduction in global terrestrial net primary production from 2000 through 2009. Science 329 (5994), 940–943.
Zhu, Q., Li, F., Riley, W.J., Xu, L., Zhao, L., Yuan, K., Wu, H., Gong, J., Randerson, J.T., 2021. Building a machine learning surrogate model for wildfire activities within a global earth system model. Geosci. Model Dev. Discuss. 1–22.
Zhu, Q., Riley, W.J., Tang, J., Koven, C.D., 2016. Multiple soil nutrient competition between plants, microbes, and mineral surfaces: model development, parameterization, and example applications in several tropical forests. Biogeosciences 13 (1), 341–363.
Zhu, Q., Zhuang, Q., 2014. Parameterization and sensitivity analysis of a process-based terrestrial ecosystem model using adjoint method. J. Adv. Model. Earth Syst. 6 (2), 315–331.
Zhu, Q., Zhuang, Q., 2015. Ecosystem biogeochemistry model parameterization: do more flux data result in a better model in predicting carbon flux? Ecosphere 6 (12), 1–20.